Hybrid turbulence models for flows around a stationary smooth circular cylinder

Jiawei He [a,b], Wentao Wang [a,c], Weiwen Zhao [a], Decheng Wan [a,*]

[a] *Computational Marine Hydrodynamics Lab (CMHL), School of Naval Architecture, Ocean and Civil Engineering, Shanghai Jiao Tong University, Shanghai, 200240, China*
[b] *Naval Research Institute (NVRI), Beijing, 100161, China*
[c] *China Ship Scientific Research Center, Wuxi, 214082, China*

ABSTRACT

The aim of this paper is to evaluate the accuracy, stability and efficiency of the different hybrid turbulence models via the benchmark computations of flows around a stationary smooth circular cylinder. The hybrid turbulence models have been validated and applied a lot in turbine flow, combustion, aerodynamic and aero-acoustic problems, while not much in hydrodynamic problems. In order to verify the simulation performance of the newly proposed hybrid strategies, this paper uses the SST-PANS, SST-SAS and SST-IDDES to compare the numerical simulation of the large separation flow problem. The model performance is assessed by a detailed comparison of predictions regarding the turbulence characteristics, the hydrodynamic characteristics, and the distribution of eddy-viscosity. The self-developed CFD solver, vim-FOAM-SJTU, is used in the present simulations. From the assessment, it is confirmed that the hybrid models have the abilities to calculate the small-scale motions, and all models can be employed to predict the unsteady characteristics of wake vortices advantageously. Both the SST-PANS and SST-IDDES models can capture complex flow structures and physics mechanism. The SAS model using the L_{vk} scale with features of local-adaptive and grid-independent can predict the eddy-viscosity reasonable. When the constant $C_s = 0.11$ contained in the L_{vk} limiter is modified to be $C_s = 0.08$, SST-SAS is also able to achieve better performance in the same mesh. The hybrid model can calculate and simulate the 3D vortex structure well, which is closer to the real physical phenomenon. And SST-IDDES has the best simulation results. The numerical results from SST-IDDES show its comparable capabilities for simulation of massively separated hydrodynamic flows and its potential application in the prediction of industrial turbulent flows for vortex-induced motions (VIM).

1. Introduction

With the development of offshore oil industry in deep sea, the phenomena of vortex-induced motions (VIM) is becoming a noteworthy issue for column-stabilized floating platforms, mainly due to its substantial fatigue damage to risers and mooring system. A clear understanding of the mechanism of VIM is essential to the security of floating platforms. Flow past a stationary smooth cylinder is a starting point to understand the VIM phenomena. Flow separation over smooth circular cylinder occurs in many engineering applications. Due to its frequent occurrence in engineering applications such as deep-sea platforms, the problem of large separation flow has always been a hot spot in turbulence theory research, and the flow around a cylinder is regarded as the most representative case. Although the geometry of the cylinder is usually simple, the flow around the cylinder still has complex flow characteristics, such as boundary layer separation and periodic vortex shedding. This brings challenges to how to use economic calculation costs to accurately predict.

The solution of turbulence becomes a bottleneck problem affecting the accuracy of numerical calculation when it is analyzed and calculated by numerical simulation methods. For a long time, the Reynolds Time Average Equation (RANS) has been the mainstream model for simulating turbulence problems in the industry due to its low calculation cost and relatively reliable calculation results. With the development of computer hardware, the rougher time-average results provided by RANS have no longer been satisfied. At the same time, although the direct numerical simulation (DNS) method can provide more accurate

---

* Corresponding author.
E-mail address: dcwan@sjtu.edu.cn (D. Wan).

Nomenclature

Re	Reynolds number based on diameter
St	Strouhal number
κ	constant value of Von Karman
U_0	freestream velocity [m/s]
$\overline{u}$	mean stream-wise velocity [m/s]
$\overline{v}$	mean crossflow velocity [m/s]
D	the diameter of the cylinder. [m]
L_z	the spanwise length of the cylinder [m]
$C_d(t)$	non-dimensional drag force coefficient
$C_l(t)$	non-dimensional lift force coefficient
$\overline{C_d}$	mean drag coefficient
C_p	pressure coefficient
C_{pb}	base pressure coefficient
C_s	Smagorsinky constant
C_{l-rms}	root mean square of lift coefficient
θ	separation angle
k	Turbulent kinetic energy
ω	specific dissipation rate
x, y, z	Cartesian coordinates [m]
Δt	Time step
f_n	Vortex shedding frequency [Hz]
T_n	Vortex shedding frequency period [s]
μ	Dynamic viscosity [kg/ms]
ρ	Fluid density [kg/m]
g	Acceleration of gravity
$\widetilde{f}_d$	The mixed weighting function
Δ	The grid scale
f_k	Spatial constant value of PANS model
τ_w	The wall stress
y^+	Y-plus, measurement of the first grid near the cylinder
VIM	vortex -induced motions (VIM)
RANS	Reynolds Time Average Equation (RANS)
SST	Shear Stress Transport (SST)
DNS	direct numerical simulation (DNS)
LES	Large Eddy Simulation(LES)
PANS	Partially Averaged Simulation(PANS)
SAS	Scale Adaptive Simulation(SAS)
DES	Detached Eddy Simulation (DES)
DDES	Delay Detached Eddy Simulation (IDDES)
IDDES	Improved Delay Detached Eddy Simulation (IDDES)

calculation results and flow field details, the computational cost of DNS method is always beyond the industry's ability to afford. Among many turbulence models, the hybrid RANS/LES method, which takes into account the computational accuracy and resource consumption, has been favored.

The hybrid model combines the advantages of RANS and LES, using RANS to calculate the laminar flow area near the wall and LES to calculate the separated flow area on the far wall(Menter et al., 2003). In recent years, a wide variety of hybrid methods have been developed by different scholars, including IDDES (Improved Delay Detached Eddy Simulation) method, SAS (Scale Adaptive Simulation) method, PANS (Partially Averaged Simulation) method, and so on. Spalart, the originator of the DES model, predicted in 2000 that the computational power of computers would be sufficient to solve 90% of turbulence problems using LES around 2045. Therefore, at this stage, the validation and development of the RANS/LES methods are still very necessary(Spalart, 2000).

The Detached Eddy Simulation (DES) method is the earliest hybrid method, which has been developed more maturely after a series of improvements (DDES, IDDES)(Heinz, 2020). The DES method is the most commonly used hybrid RANS/LES method(Shur et al., 2008). Its calculation formula is simple, and it is also adaptable to complex geometric shapes. However, the original DES method has some problems. One of the most serious problems facing DES is stress mode loss (MSD) (Menter, 1994). When the stress mode loss occurs, the grid in the boundary layer area that should be calculated by RANS is so fine that the LES is activated, but in fact it still cannot meet the LES simulation requirements. At this time, the calculation will produce grid-induced non-physical flow separation, which makes the calculation result of DES even inferior to the calculation result using RANS. It is against logic to degrade the calculation results because of the refinement of the grid. The Delayed Detached Eddy Simulation (DDES) protects the RANS area from being switched to the LES area prematurely by optimizing the characteristic turbulence length scale of the DES, thereby effectively solving the MSD problem(D'Alessandro et al., 2016). Nevertheless, the DDES model is still room for improvement. Charles Mockett (Mockett et al., 2010) used DES turbulence model to simulate the flow around cylinder at a high sub-critical Reynolds number (Re = 1.4×10^5). Good comparability with PIV experimental field data is facilitated by the clearly defined geometry, although some uncertainty remains regarding

the free stream turbulence intensity. Krishnan (Krishnan et al., 2006) used DDES to predict the massively separated flow around a circular at Reynolds numbers based on the cylinder diameter and freestream velocity of 1.4×10^5 and 8×10^6.

The other problem of traditional DES method is the "gray zone" problem where the behavior of the RANS and LES regions is unknown. The "gray zone" problem has been difficult to solve, which is a hot research topic. The implantation method is considered as one of the effective means to solve "gray zone" problem, So far, academic research on implantation methods has focused on how to reconstruct and transfer appropriate turbulence information at the RANS/LES interface. The difficulty comes from two aspects: on the one hand, how the LES can transmit appropriate boundary information to the RANS region where statistical averaging is performed; on the other hand, how the RANS, which lacks non-constant information such as turbulent pulsations, can transmit sufficient turbulent pulsations to the LES, which requires that the pulsations provided by the RANS are comparable to the real situation but not too costly to compute. The EU Go4Hybird (Mockett et al., 2015) project is a more detailed and systematic study of implantable methods; Shur et al. (2011) first proposed a cyclic turbulence technique for implantable methods, followed by the development of a synthetic turbulence technique for implantable methods (Shur et al., 2014), which made a considerable contribution to the development of implantable methods.

The scale-adaptive simulation (SAS) was proposed by Menter (Menter et al., 2003). The SAS model is a new generation of non-constant turbulence prediction method that can resolve broad-frequency non-constant turbulent pulsations with less dependence on the computational grid, which can reasonably release more flow field information by adding the von Karman length scale with reference to the local flow. The SAS model solves the Reynolds Averaged Navier-Stokes equations in stable flow regions. In unstable flow regions, the SAS models reducing eddy viscosity according to the locally resolved vortex size, which represented by reducing the von Karman length scale (Stamou and Papadonikolaki, 2014). The partially averaged Navier-Stokes (PANS) model is also a recently developed RANS-DNS bridging model, which is relatively simple to construct and adjusts the turbulence modulation by adding the modulated turbulence energy scaling parameter f_k to adjust the turbulence solution scale(Razi, 2017). The PANS model was developed to overcome the grid dependency

associated with the customary implementation of the hybrid method.

The turbulence models (SST-PANS,SST-SAS and SST-IDDES) have been validated and applied a lot in turbine flow (Krappel et al., 2015), Combustion(Lysenko et al., 2012),Aerodynamic and Aeroacoustic(Shur et al., 2014) problems, while not much in hydrodynamic problems. In order to systematically verify the simulation performance of the hybrid turbulence models, this paper uses the SST-PANS,SST-SAS and SST-IDDES to compare the numerical simulation of the large separation flow problem. The large-separated flow calculation examples adopted in this paper are the flow around a cylinder with Reynolds number Re = 3900. The example is considered to be standard example for testing the performance of the turbulence model. The focus is on capturing the flow field characteristics, calculating hydrodynamic characteristics. By comparing the calculation results of different hybrid methods to the grid, and the adjustment mechanism of the scale function of the hybrid models on the flow field is discussed.

The primary objective of this paper is to assess the performance of these newly implemented approaches in a production CFD code to solve hydrodynamic problems.

The paper is organized as follows: section 2 describes the discretization format and the main formula of the selected turbulence models, whereas section 3 introduces the numerical case setup and the overall computational grid used to execute the simulation. The results are then presented and discussed in section 4. Finally, conclusions are provided in section 5.

2. Numerical methods

2.1. Discretization format

In the present study, the governing equations are discretized using a finite volume method for solving the incompressible Navier–Stokes equations using inhouse solver vim-FOAM-SJTU, with newly implemented hybrid turbulence models. The suitability of the present solver has been clarified by Zhao et al. for solving flow past two circular cylinders in tandem(Zhao and Wan, 2016)and simulating vortex-induced motions of a semi-submersible(Zhao et al., 2018). The time discretization is done using second order implicit Euler scheme. A second order Gauss integration is used for spatial gradient calculations. The convection operator is discretized using a total variation diminishing (TVD) scheme. The merged PISO-SIMPLE (PIMPLE) algorithm is used for solving the coupled pressure–velocity equations.

2.2. Turbulence model

2.2.1. $k - \omega$ SST model

The SST model(Menter, 1994) is modified by mixing the standard k-ω model with the k-ε model, which takes into account the near-wall performance of the k-ω model and the far-field accuracy of the k-ε model. The transport equations for turbulent kinetic energy k and specific dissipation rate ω in the SST model can be expressed as follows.

$$\frac{\partial \rho k}{\partial t} + \nabla \cdot (\rho U k) = P_k - \beta^* \rho k \omega + \nabla \cdot [(\mu + \sigma_k \mu_t) \nabla k] \tag{1}$$

$$\frac{\partial \rho \omega}{\partial t} + \nabla \cdot (\rho U \omega) = \frac{\alpha}{v_t} P_k - \beta \rho \omega^2 + \nabla \cdot [(\mu + \sigma_\omega \mu_t) \nabla \omega] \\ + (1 - F_1) \frac{2\rho \sigma_{\omega 2}}{\omega} \nabla k \nabla \omega \tag{2}$$

Where the model parameters $\beta^* = 0.09$, $\gamma_1 = 5/9$, $\gamma_2 = 0.44$, $\beta_1 = 0.075$, $\beta_2 = 0.0828$, σk1 = 0.85, σk2 = 1.0, σω1 = 0.5, σω2 = 0.0828.

2.2.2. SST-SAS

The Scale-Adaptive Simulation (SAS) model is a relatively new and innovative turbulence model that uses the von Karman length scale L_{vk}, which portrays the local flow topology, as a second length scale in the turbulence model. The SAS model based on the SST model is constructed by adding the source term Q_{SAS} to the ω equation of the SST model, the details of transport equations are defined by:

$$\frac{\partial \rho k}{\partial t} + \nabla \cdot (\rho U k) = P_k - \rho C_\mu k \omega + \nabla \cdot [(\mu + \sigma_k \mu_t) \nabla k] \tag{3}$$

$$\frac{\partial \rho \omega}{\partial t} + \nabla \cdot (\rho U \omega) = \frac{\alpha}{v_t} P_k - \beta \rho \omega^2 + Q_{SAS} + \nabla \cdot [(\mu + \sigma_\omega \mu_t) \nabla \omega] \\ + (1 - F_1) \frac{2\rho \sigma_{\omega 2}}{\omega} \nabla k \nabla \omega \tag{4}$$

Q_{SAS} which is defined by:

$$Q_{SAS} = max\left[\rho \xi \kappa S^2 \left(\frac{L}{L_{vk}} \right)^2 - C \cdot \frac{2\rho k}{\sigma_\varphi} max\left(\frac{|\nabla \omega|^2}{\omega^2}, \frac{|\nabla k|^2}{k^2} \right), 0 \right] \tag{5}$$

Where, S is invariant measure of the strain rate tensor, defined as $S = \sqrt{2 S_{ij} S_{ij}}$, and $S_{ij} = \frac{1}{2} \left(\frac{\partial u_i}{\partial x_j} + \frac{\partial u_j}{\partial x_i} \right)$, the constants in the equation are: $C = 2.0$, $\xi = 3.51$, $\kappa = 0.41$, $\sigma_\varphi = \frac{2}{3}$, $C_\mu = 0.09$. The turbulence scale $L = \sqrt{k}/(C_\mu^{1/4} \cdot \omega)$, and the von Karman length scale is $L_{vk} = max\left(\frac{\kappa S}{|\nabla^2 U|}, \right.$ $\left. C_s \sqrt{\kappa \zeta_2 / ((\beta/C_\mu) - \alpha)} \cdot \Delta \right)$. All the coefficients and the details can be found in the paper (Menter and Egorov, 2010). The value of the Smagorsinky constant is $C_s = 0.11$.

It can be seen from Equation (5) that a length scale term L_{vk}, determined by the first and second-order velocity derivatives, appears in the SAS model, which is based on the local flow and independent of the grid scale. Within the turbulent boundary layer, L_{vk} can modulate all turbulent pulsations in the inertial subregion, while in the unsteady region L_{vk} can adjust the RANS length scale according to the local grid-resolved turbulent vortex dynamics. In the SAS model, the turbulent viscosity μ_t is still calculated according to equation $\mu_t = \frac{\alpha_1 \rho k}{max(\alpha_1 \omega, SF_2)}$.

2.2.3. SST-PANS

The strategy for the hybridization of SST-PANS turbulence model is very different from the DES approaches. The SST-PANS is a coefficient method, which focus on the modification of model coefficients in RANS equations so that resolving modes can be generated. The details of SST-PANS model have been presented and evaluated for flow around cylinder by Elmiligui et al., and the model gives good agreement with the experiment results(Elmiligui et al., 2004; Pereira et al., 2018).

$$\frac{\partial (\rho k_u)}{\partial t} + \frac{\partial (\rho U_i k_u)}{\partial x_i} = \widetilde{P}_{ku} - \beta^* \rho k_u \omega_u + \frac{\partial}{\partial x_i} \left[(\mu + \sigma_{ku} \mu_u) \frac{\partial k_u}{\partial x_i} \right] \tag{6}$$

$$\frac{\partial (\rho \omega_u)}{\partial t} + \frac{\partial (\rho U_i \omega_u)}{\partial x_i} = \frac{\gamma}{v_u} \widetilde{P}_{ku} - \beta' \rho k_u \omega_u^2 + \frac{\partial}{\partial x_i} \left[(\mu + \sigma_{\omega u} \mu_u) \frac{\partial \omega_u}{\partial x_i} \right] \\ + 2(1 - F_1) \frac{\rho \sigma_{\omega 2u}}{\omega_u} \frac{\partial k_u}{\partial x_i} \frac{\partial \omega_u}{\partial x_i} \tag{7}$$

Where,

$$\beta' = \gamma \beta^* - \frac{\gamma \beta^*}{f_\omega} + \frac{\beta}{f_\omega}; \sigma_{ku} = \sigma_k \frac{f_\omega}{f_k}; \sigma_{\omega u} = \sigma_\omega \frac{f_\omega}{f_k} \tag{8}$$

Where, $\beta^* = 0.09$, $\gamma_1 = 5/9$, $\gamma_2 = 0.44$, $\beta_1 = 0.075$, $\beta_2 = 0.0828$, σk1 = 0.85, σk2 = 1.0, σω1 = 0.5, σω2 = 0.0828.

$$f_k = \frac{k_u}{k}; f_\omega = \frac{\omega_u}{\omega} = \frac{f_\varepsilon}{f_k} \tag{9}$$

Where, k is the turbulent kinetic energy and ω is the specific dissipation rate, respectively.

The expressions for the two blending functions in the case of SST-PANS are given by:

$$F_1 = \tanh\left\{\min\left\{\left[\max\left(\frac{\sqrt{k_u}}{\beta^*\omega_u d}, \frac{500\mu}{d^2\rho\omega_u}\right), \frac{4\rho\sigma_{\omega 2u}k_u}{CD_{k\omega}d^2}\right]\right\}^4\right\} \tag{10}$$

$$F_2 = \tanh\left\{\left[max\left(\frac{2\sqrt{k_u}}{\beta^*\omega_u d}, \frac{500\mu}{d^2\rho\omega_u}\right)\right]^2\right\} \tag{11}$$

Where, the coefficient $CD_{k\omega} = \max\left(\frac{2\rho\sigma_{\omega 2u}}{\omega_u}\frac{\partial k_u}{\partial x_i}\frac{\partial \omega_u}{\partial x_i}, 10^{-10}\right)$.

The unresolved eddy viscosity μ_u is defined as:

$$\mu_u = min\left(\frac{\rho k_u}{\omega_u}, \frac{\rho a_1 k_u}{SF_2}\right) \tag{12}$$

In the early applications of the PANS model, f_k was usually set as a spatial constant value. But it is not appropriate to use the same constant value of f_k for the entire flow field through the calculations. In this work variable f_k as a function of the grid scale Δ and the turbulence scale l_u as follows.

$$f_k = min\left[C_{PANS}\left(\frac{\Delta}{l_u}\right)^{\frac{2}{3}}, 1\right]; l_u = \frac{\sqrt{k_u}}{\beta^*\omega_u} \tag{13}$$

Where all other coefficients depend on the reference(Ye et al., 2020).

2.2.4. SST-IDDES

In the Delayed Detached Eddy Simulation (DDES), the turbulent length scale is determined using information from the eddy viscosity field, in addition to the wall distance and grid spacing. SST-DDES utilizes sub-grid scale model to handle the flow in the free shear flow area far away from the wall, and RANS's SST model is used to solve the flow in the boundary layer near the wall and other areas. This can guarantee the accuracy of LES solution, but also reduce the amount of calculation in the near-wall region of the boundary layer. The turbulence model applied to the calculations was the IDDES. The IDDES was presented as an improvement of the DDES in reference(Gritskevich et al., 2012).

The simplified version of IDDES length scale is as follows:

$$l_{IDDES} = \widetilde{f}_d d + \widetilde{f}_d(1 - \widetilde{f}_d)\psi C_{DES}\Delta \tag{14}$$

Where, $\widetilde{f}_d$ is mixed weighting function $\widetilde{f}_d = \max\{f_B, 1 - f_{dt}\Delta\}$.

The LES length-scale Δ is defined as:

$$\Delta = min\{C_w max[d_w, h_{max}], h_{max}\} \tag{15}$$

$$f_{dt} = 1 - \tanh\left[(C_{dt1} r_{dt})^{C_{dt2}}\right] \tag{16}$$

$$r_{dt} = \frac{\nu_t}{\kappa^2 d_w^2\sqrt{0.5\cdot(S^2 + \Omega^2)}} \tag{17}$$

$$f_B = min\left\{2e^{-9\alpha^2}, 1.0\right\} \tag{18}$$

$$\alpha = 0.25 - d_w/h_{max} \tag{19}$$

The following constants are introduced in the model: $C_w = 0.15$, $C_{dt1} = 20, C_{dt2} = 3$. Where all other coefficients depend on the reference (Gritskevich et al., 2012).

2.3. Near-wall treatments

For the turbulence kinetic energy k, the "*kqRWallFunction*" boundary condition is used, which means a zero-gradient condition of k on the wall. For the specific turbulence dissipation ω, the "*omegaWallFunction*" boundary condition s is used and expressed as Equation (20).

$$\omega = \sqrt{\omega_{vis}^2 + \omega_{log}^2} \tag{20}$$

in which, ω_{vis} and ω_{log} are ω in viscous and logarithmic regions,

respectively. And the ω_{vis} and ω_{log} are expressed as Equation (21).

$$\omega_{vis} = \frac{6\nu}{0.075(y^+)^2}; \omega_{log} = \frac{1}{0.3\kappa}\frac{u_\tau}{y^+} \tag{21}$$

For the turbulent viscosity, the *nutUSpaldingWallFunction* is chosen. It gives a continuous profile to the wall according to Spalding's law as Equation (22).

$$y^+ = u^+ + \frac{1}{9.8}\left[e^{\kappa u^+} - 1 - \kappa u^+ - 0.5(\kappa u^+)^2 - \frac{1}{6}(\kappa u^+)^3\right] \tag{22}$$

Where κ is a constant value of Von Karman.

3. Case setup

3.1. Computational domain

The simulations are performed on an O-grid, with a computational domain extending $45D$ in the length,$30D$ in the width and πD in the spanwise length, where D is the diameter of the cylinder. The full computational domain is shown in Fig. 1. As pointed out by the reference (Khan et al., 2019) that the spanwise length L_z has a negligible effect on calculating results, so the spanwise length L_z is πD in present simulation. As the reference (Wissink and Rodi, 2008) pointed out, increasing the spanwise size of the computational domain from $L_z = 4D$–$8D$ was found to only marginally affect the profiles of turbulence statistics in the wake of the cylinder.

The boundary conditions used for the numerical simulations can be defined as follows. Velocity will be assigned as fixed value $u_x = U_0$, $u_y = u_z = 0$, in the inlet. On the cylinder boundary no slip condition for the velocity will be applied. The pressure boundary condition in inlet is of a type zero gradient on the cylinder. At the outlet boundary, the pressure gradient is set equal to 0. The rest of the boundaries is defined as symmetry boundary for the reason of assuming that the height of the cylinder is infinite.

3.2. The simulation grids

We use 3 sets of grids to analyze the convergence of the grids. The 3 sets of grids have the same number of grids in vertical direction. The
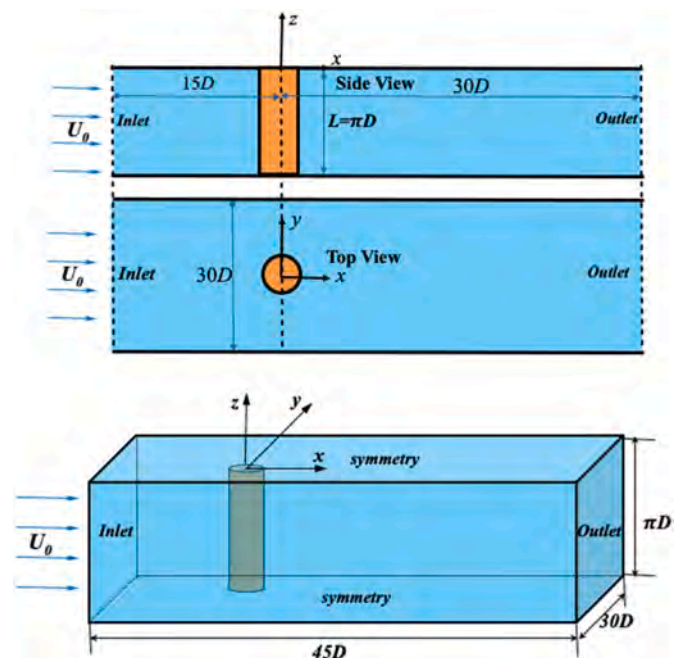

Fig. 1. Computational domain and boundary conditions.

difference between each set of grids is mainly the area around the cylinder on the cross section, see the Fig. 2. The simulation cases are shown in Table 1.The details of the three sets of grids are shown in Table 2. The mean drag coefficient $\overline{C_d}$ and root mean square of lift coefficient $C_{l\text{-}rms}$ in Table 2, which is calculated from Case B.The number of distributed grid layouts and the distance between the first layer of grids and the near-wall surface are analyzed by increasing or decreasing the density of the grid to analyze the effect of spatial dispersion on the calculation results.

Details of the refinement mesh around the cylinder is shown in Fig. 3. The wall y^+ values is below 1, indicating sufficient resolution in the near boundary layer for the simulation. The total grid number for the present simulation is around 4.2 million. The time step of the simulation is selected based on the local Courant–Friedrichs–Lewy criteria (CFL number $= U_0\Delta t/\Delta x$) that should not exceed 0.5 to ensure the convergence of the solution. Infact, in most of the time CFL number varied in between 0.4 and 0.5 during the present simulations. The non-dimensional time step is taken as $\Delta t = 0.001$, which is found to be sufficient to capture the unsteady characteristics of the flow.

Computations are carried out in parallel on Intel Xeon (E5-2650 v4 CPU). The workload is distributed into 48 processors on a Linux cluster

Table 1
Simulation cases.

Case	Turbulence Model	Flow velocity (m/s)	Re	Δt	Total cell numbers
Case A	$k - \omega$ SST	0.39	3900	0.001	4,250,000
Case B	SST-PANS	0.39	3900	0.001	4,250,000
Case C	SST-DES	0.39	3900	0.001	4,250,000
Case D	SST-IDDES	0.39	3900	0.001	4,250,000
Case E	SST-SAS	0.39	3900	0.001	4,250,000
Case F	Smagorinsky LES	0.39	3900	0.001	4,250,000

(a) Mesh I (G1)

(b) Mesh II (G2)

(c) Mesh III (G3)

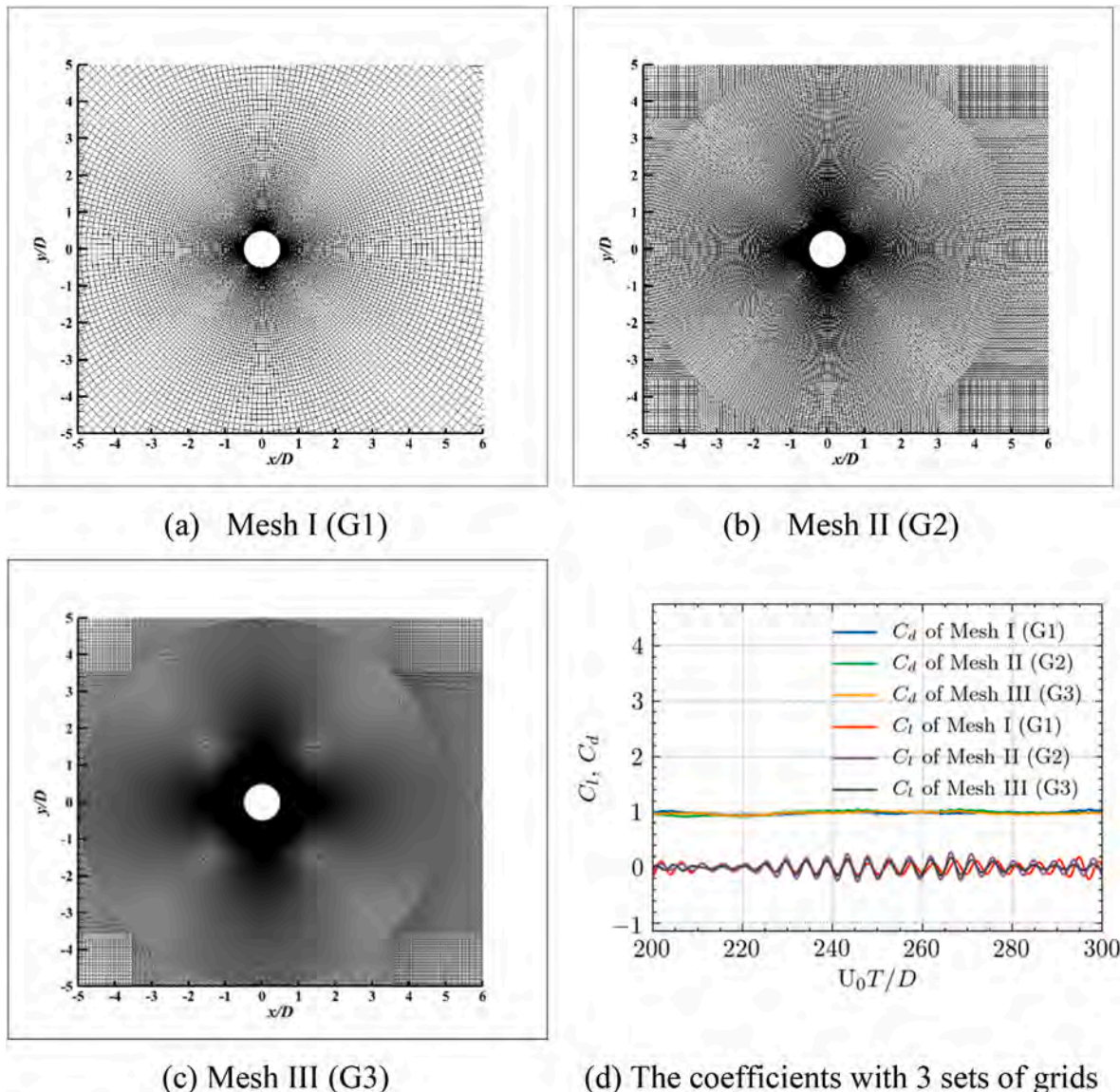(d) The coefficients with 3 sets of grids

Fig. 2. The details of the mesh at cross section for the computation.

Table 2
The details of the three sets of grids.

Grid	Total cell numbers	L_z	Number of Nodes around the cylinder	The height of nearest grid to the cylinder boundary	$\overline{C_d}$	$C_{l\text{-}rms}$	St
G1	2,190,000	πD	60×60	$0.005\ D$	0.921	0.106	0.21
G2	4,250,000	πD	120×120	$0.003\ D$	0.953	0.078	0.21
G3	6,160,000	πD	200×200	$0.002\ D$	0.951	0.074	0.21

for calculation, and the total computational cost is around 1152 CPU hours for each computation.

3.3. Simulation results

3.3.1. Validation

As shown in Table 3, the calculated average drag coefficient $\overline{C_d}$, leeward pressure coefficient C_{pb}, Strohal number St, separation angle θ, and recirculation length L_{rec} are in good agreement with the experimental results, which verifies the accuracy of the simulation method of flow around cylinder. The error of present hybrid models and the LES model is small, which is within the reasonable range of the experimental value. Meanwhile, the deviation of the separation angle, the mean recirculation length and the minimum mean flow velocity by $k-\omega$ SST

RANS method is relatively large.

3.4. The forces coefficient

3.4.1. Spectra of lift coefficient

The power spectrum of the vortex shedding frequency obtained by the Fourier transform (FFT) of the lift coefficient history time curve is given in Fig. 4, from which the vortex shedding frequency f_n and the Strohal number St (St $= f_n D/U_0$) can be calculated. The vortex shedding frequency f_n, period T_n and Strohal number St of each model are shown in Table 4. Fig. 5 demonstrates the time histories of lift coefficient (C_l) by present simulation of different turbulence models.

3.4.2. The drag force coefficient

Fig. 6 demonstrates the time histories of drag coefficient (C_d) by present simulation using different turbulence models. It is interesting that the magnitudes of the drag coefficients C_d obtained by the hybrid models were significantly lower than those predicted by the conventional RANS model.

3.5. Velocity and pressure

3.5.1. The velocity field

Fig. 7 shows contour and streamlines of mean velocity onto a horizontal plane, simulated by different models. We notice that the
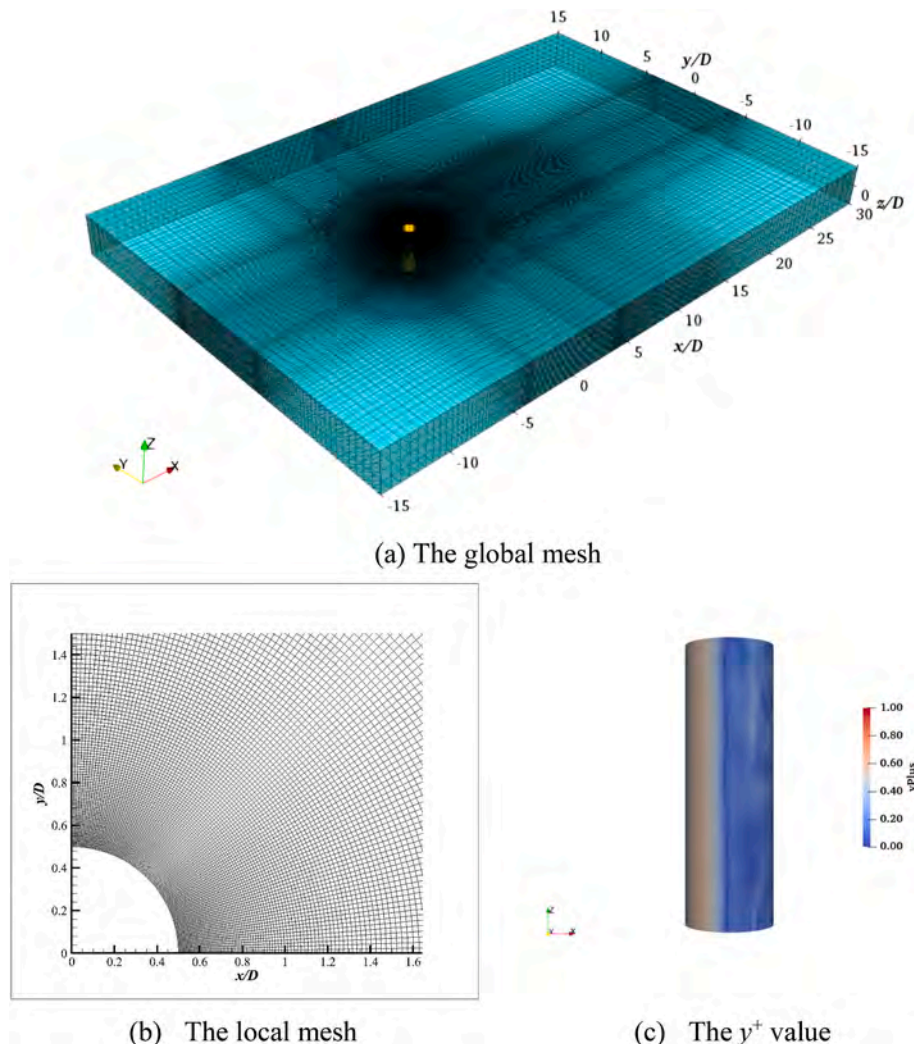

(a) The global mesh

(b) The local mesh

(c) The y^+ value

Fig. 3. Details of the mesh around cylinder and y^+ value of Mesh II (G2).

Table 3

Comparison the coefficients with experimental and literature calculations, Reynolds number(Re) Re = 3900.

Model	$\overline{C_d}$	$-\overline{C_{pb}}$	St	L_{rec}/D	θ	U_{min}/U_0
Exp. of (Lourenco, 1994)	0.99	0.88	0.215	1.19	86	0.24
SST-DES of Ref. (Xu et al., 2007)	1.08	–	0.220	0.98	–	–
DNS of Ref. (Frederic, 2002)	1.03	0.93	0.220	1.30	85.7	–
LES of Ref. (Frederic, 2002)	1.14	0.99	0.210	1.04	87.3	–
LES of Ref. (Kravchenko, 2000)	1.04	0.94	0.210	1.35	88.0	0.37
Present $k-\omega$ SST	1.24	1.25	0.216	0.52	91.1	0.07
Present SST-PANS (Variable f_k)	0.95	0.88	0.216	1.67	87.2	0.23
Present SST-DES	0.99	0.84	0.213	1.56	86.7	0.29
Present SST-IDDES	0.97	0.87	0.216	1.34	86.5	0.28
Present SST-SAS (C_s = 0.11)	1.07	0.85	0.213	1.45	87.9	0.28
Present Smagorinsky LES	0.97	0.89	0.210	1.27	88.9	0.23

shortening of the recirculation length obtained by our $k-\omega$ SST computations as compared to other hybrid models and the DNS result by Frederic et al. (Frederic, 2002). We note once again the shorter recirculation bubble of the LES computations by Frederic (2002).

3.5.2. The pressure coefficient

The pressure coefficient C_p is defined as following:

$$C_p = \frac{p - p_\infty}{0.5U^2} \tag{23}$$

in which, p is the pressure, p_∞ is the reference pressure, U is the velocity of current. τ_ω is related to the wall shear stress on cylinder surface.

The distributions of normalized pressure coefficient Cp around the surface of the cylinder compared with the experiment value is shown in Fig. 8 (a). This study shows that the results are in good agreement with the experimental results. The pressure coefficient reaches a maximum value slightly greater than 1 at the upstream stationary point, followed by a minimum value near the separation angle (about $\theta = 65°$). It can be seen that the simulation results of $k-\omega$ SST deviate the most from the

Table 4

The vortex shedding frequency f_n, period T_n and Strohal number St.

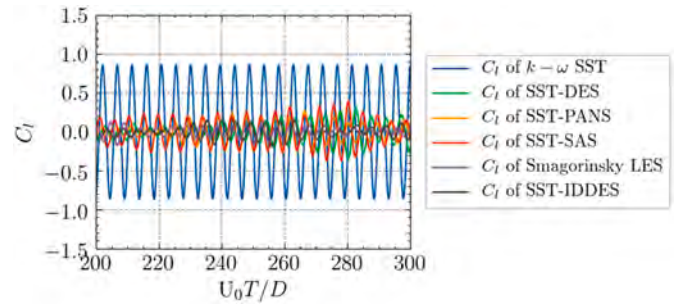| Model	f_n (Hz)	T_n (s)	St
Present $k-\omega$ SST	8.41	0.119	0.216
Present SST-DES	8.31	0.120	0.213
Present SST-PANS	8.41	0.119	0.216
Present SST-SAS	8.31	0.120	0.213
Present Smagorinsky LES	8.21	0.121	0.210
Present SST-IDDES	8.31	0.120	0.213

Fig. 5. Time history of the lift coefficient (C_l) with different models comparison.
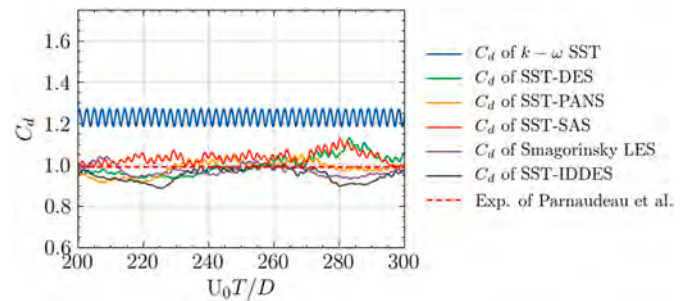

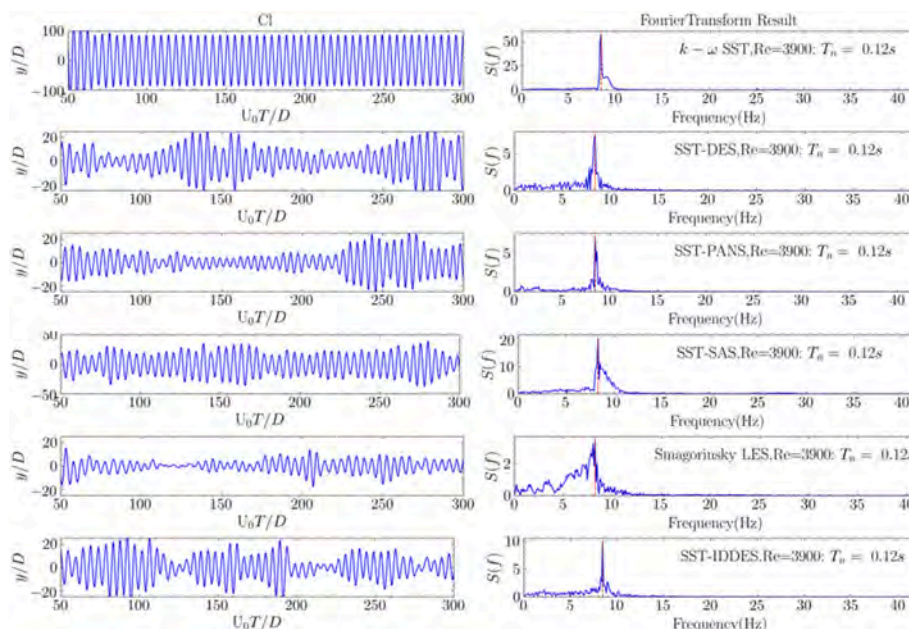**Fig. 6.** Time history of the drag coefficient (C_d) with different models' comparison.

Fig. 4. Time history curve and Fourier transform result of the lift coefficient (C_l).

(a) $k - \omega$ SST

(b) SST-DES

(c) SST-PANS

(d) SST-SAS

(e) Smagorinsky LES

(f) SST-IDDES

(g) DNS of Ref (Frederic, 2002)
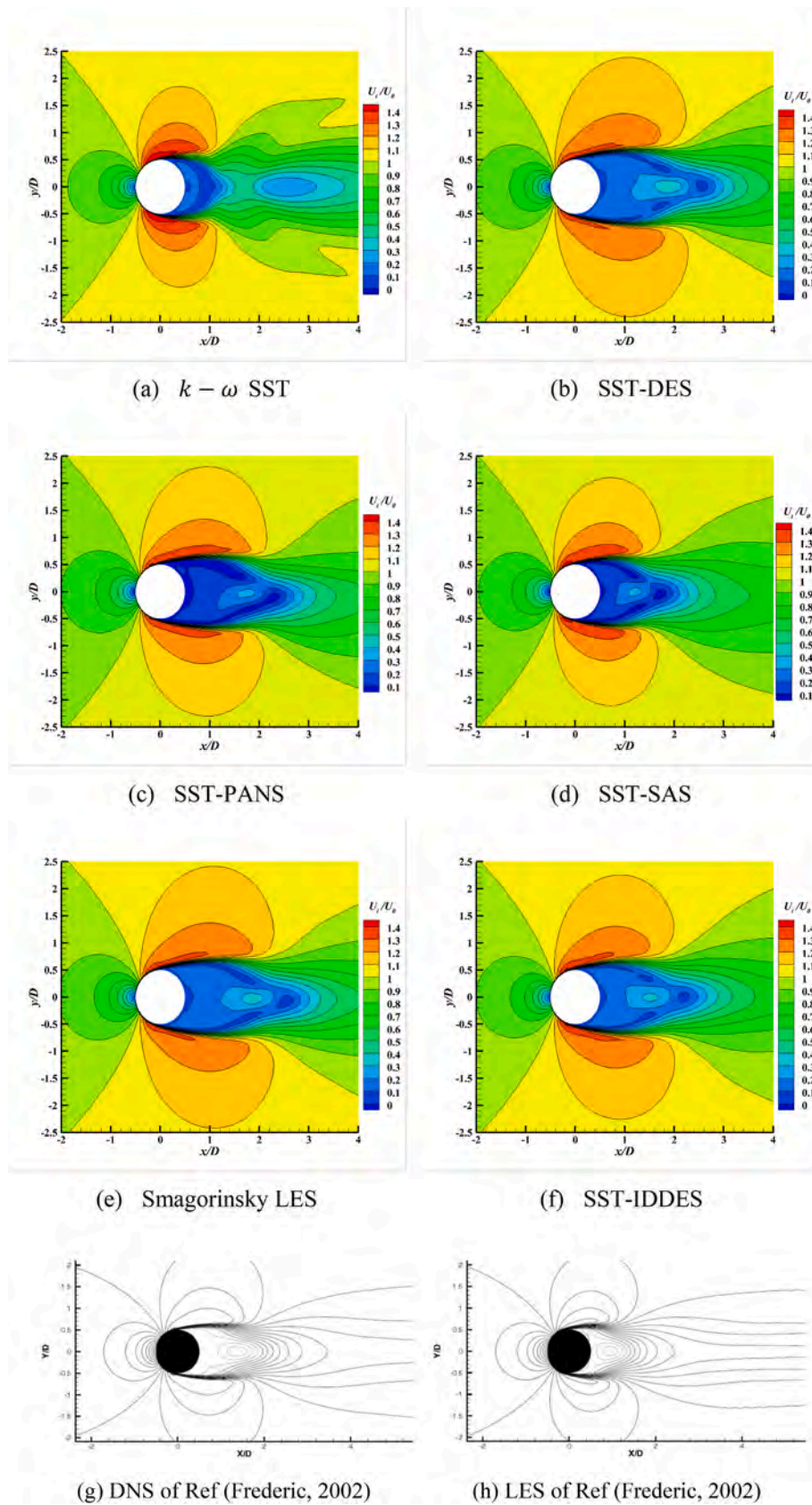
(h) LES of Ref (Frederic, 2002)

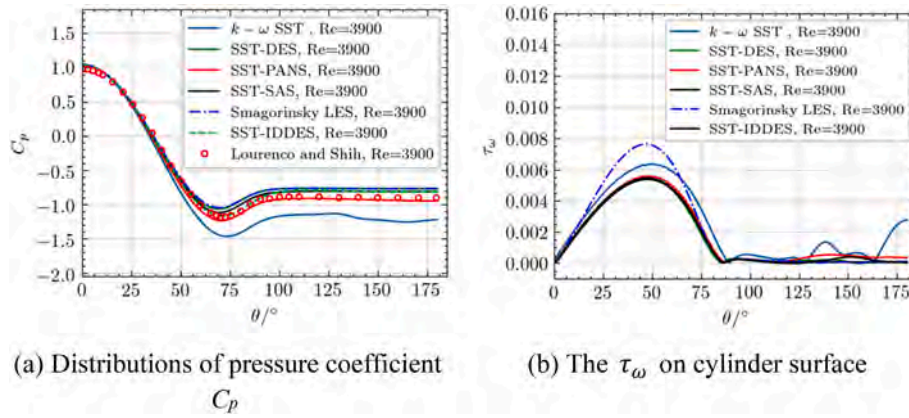**Fig. 7.** Isocontour maps of mean velocity for the flow past a cylinder in horizontal plane $z/D = 0$.

Fig. 8. Distributions of pressure on cylinder surface.(θ=0° corresponding to the front stagnation point).

experimental results. The pressure coefficient distribution curves calculated by SST-SAS, SST-DES, SST-IDDES, and LES almost coincide exactly and are all quite close to the experimental results. The results calculated by SST-PANS are slightly smaller than the other hybrid models and the LES results, but are most consistent with the experimental values. This indicates that the hybrid models are accurate for the calculation of the circumferential pressure coefficients on the cylindrical wall surface. The wallShearSress on cylinder surface is shown in Fig. 8 (b). It can be seen that the result simulated by the Smagorinsky LES method has maximum value of τ_ω.

The iso-contour maps of circumferential pressure coefficients C_p by different turbulence model is given in Fig. 9. It can be seen that the pressure reaches its maximum value at the upstream stagnation point, then is reduced down to its minimum before recovers to a constant value which is known as the base pressure C_{pb}. It is observed from the results that SAS model show a bit smaller recirculation length compared to the other models. Moreover, a slight difference is observed between the DES result and the results of IDDES by present simulation, where WMLES in IDDES will result in early transition of the separating shear layer. Overall, this study agrees with previous experiments, and the recirculation length of the hybrid models case study is consistent with the experimental results obtained by Lourenco and Shih (Lourenco, 1994).

3.6. Instantaneous vortex

According to Liu et al. (2019), the development of vortex identification methods can be classified into three generations. The first-generation methods are based on the vorticity. However, it has been found by many researchers that the correlation between the vorticity and vortices can be rather weak. The second generation of vortex identification methods, including Q, λ_2 and λ_{ci} criteria, has thus been proposed to overcomethe problems associated with vorticity-based methods. However, the second generation methods are often plagued with case-related threshold problem in actual use and prone to contamination by shearing(Gao and Liu, 2018). To overcome the threshold problem, in 2018(Tian et al., 2018), a Liutex vector (previously named Rortex) was proposed to provide a mathematical and systematical definition of the local rigid rotation part of the fluid motion, including both the local rotational axis and the rotational strength. As a new physical quantity raised by Liu et al., Liutex has direction and magnitude. Its direction represents the local vortex line and is parallel to the normal vector of the vortex iso-surface. Its magnitude is exactly the local angular speed, and Liutex represents a force which is the driving force of turbulence generation.Acorrding to Liu et al. (2019) the definition of *Omega-liutex* Ω_{Liu} is given by:

$$\Omega_{Liu} = \frac{\beta}{\beta + \alpha + \varepsilon} \tag{24}$$

Where, $\alpha = \frac{1}{2}\sqrt{\left(\frac{\partial U}{\partial X} - \frac{\partial V}{\partial Y}\right)^2 + \left(\frac{\partial V}{\partial X} + \frac{\partial U}{\partial Y}\right)^2}$, $\beta = \frac{1}{2}\left(\frac{\partial V}{\partial X} - \frac{\partial U}{\partial Y}\right)$, and ε can be defined as a function of the maximum of the term $(\beta^2 - \alpha^2)$, $\varepsilon = 0.001 \times (\beta^2 - \alpha^2)_{max}$.

3.6.1. The vortex structures

Fig. 10 shows the three-dimensional vortex structure in the wake region marked Liutex criterion Ω_{Liu}, which is coloured by the dimensionless velocit. A comparative analysis reveals that the results of $k - \omega$ SST show a two-dimensional Karman Vortex Street phenomenon and do not capture the fine broken vortex structure in the far wake region well. In contrast, the results of the hybrid turbulence model such as SST-IDDES show a clear three-dimensional effect, and the fine broken vortex structure in the far wake region is captured in the cylindrical spreading direction. Overall, at the far wake, the vortex structure simulated by RANS is larger and flatter than that of the hybrid model.

It can be seen from Fig. 10 that although SST-IDDES and SST-PANS, SST-SAS all capture the turbulent structure very well, the SST-IDDES captures the turbulent structure more finely than the other hybrid models. Near the wall, the SST-IDDES model captures a considerable number of fine vortices.

3.6.2. The vorticity

Fig. 11 shows the contours of the instantaneous vorticity for the flow past a cylinder in the horizontal plane $z/D = 0$. From the experimental and previous calculation results, it can be seen that the development of the shear layer on the cylindrical wall is very sensitive to external influences, and the small external disturbance can easily cause the early separation of the boundary layer, which makes the shear layer shorter, and then affects the measurement or calculation results of the recirculation region and the whole flow field. Fig. 11 also shows that, comparing the instantaneous ($U_0T/D = 300$) shear layer of several models of vorticity contours, it can be seen by comparison that the shear layer length relationship is: SST-PANS> LES>SST-DES>SST-IDDES>SST-SAS>SST. We could draw the conclusion that the recirculation region of the hybrid turbulence model is found to be longer than that of the RANS model. In addition, the results of the hybrid turbulence models (SST-DES, SST-SAS, SST-PANS, SST-IDDES) are irregular compared to the RANS type (SST model), where the hybrid turbulence model has many small broken vortex structures in the cylindrical far wake field, while the RANS has only regular large vortex structures with very weak 3D effects.

3.7. Discussion of result

3.7.1. Discussion of SST-SAS model

As mentioned before, it is necessary to construct a limiter of the von Karman scale L_{vk} in case that L_{vk} is smaller than local grid scale when the
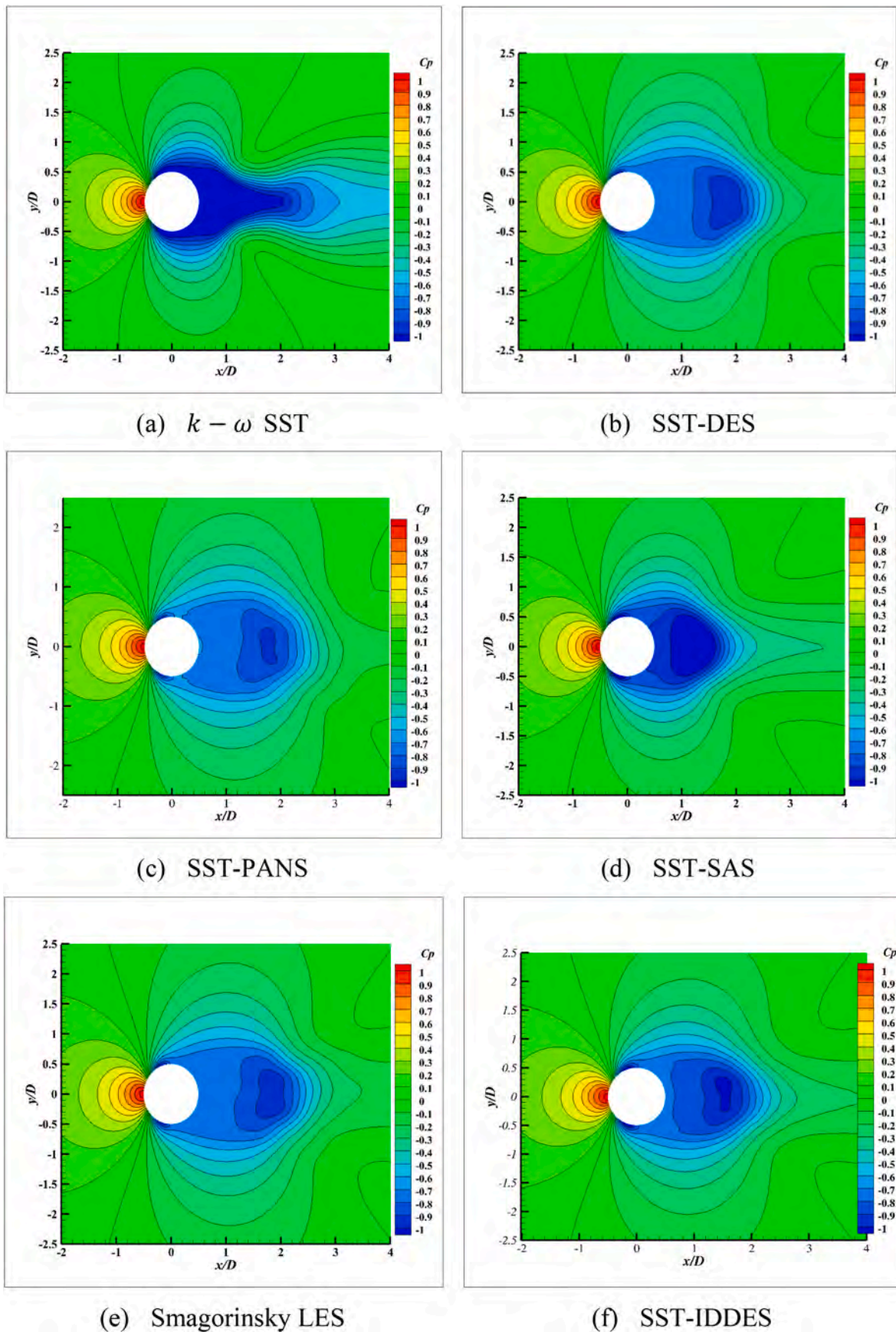
Fig. 9. Isocontour maps of circumferential pressure coefficients C_p for the flow past a cylinder in horizontal plane $z/D = 0$.
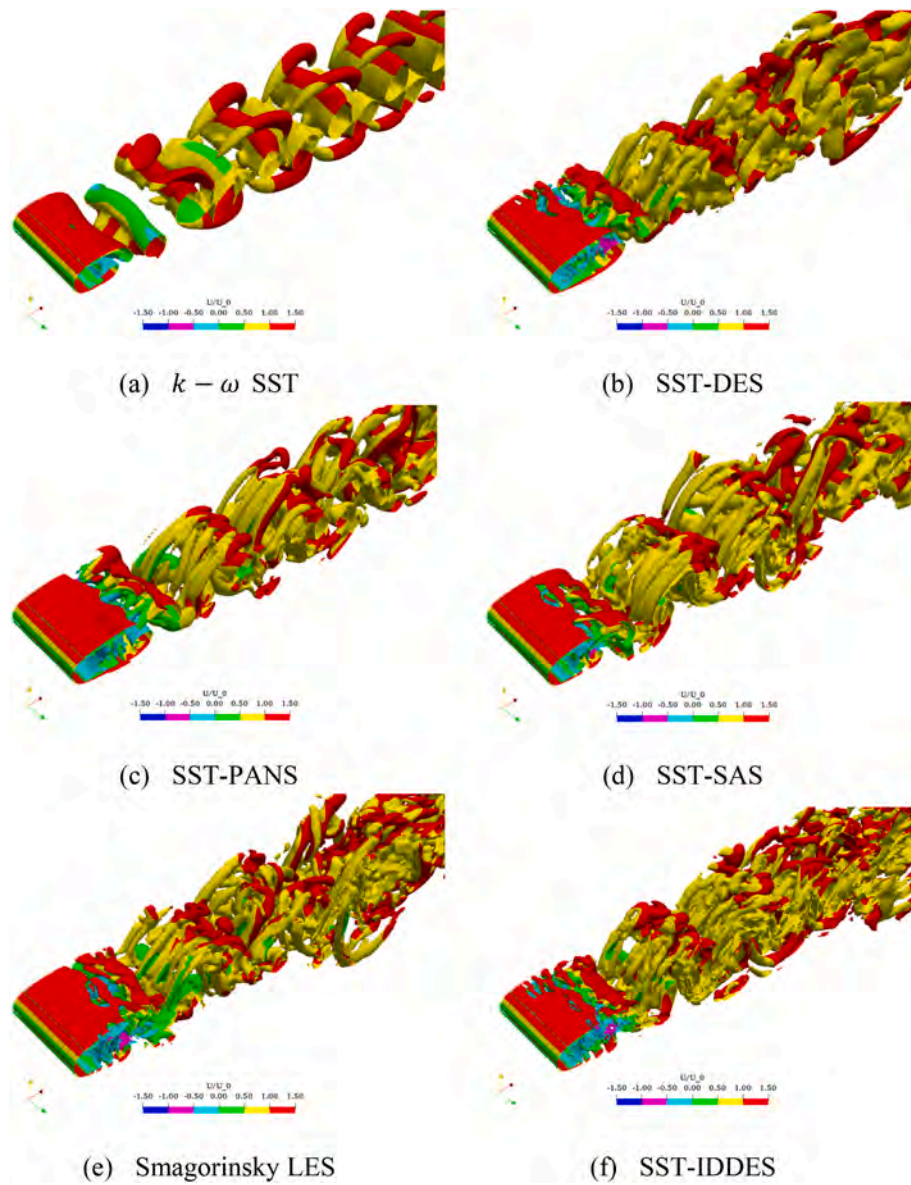
Fig. 10. Instantaneous view of coherent vortex structures contoured by using Omega-liutex $\Omega_{Liu} = 0.52$ iso-surfaces for the flow over a single cylinder at $Re = 3900$.

unsteadiness in the flowfield is quite large. Otherwise, the finest scale turbulence fluctuations which is excess the resolution of local grid will fail to be correctly dissipated. Smagorinsky model as the most classic LES model, is used to construct L_{vk} limiter with the eddy-viscosity constraint as described below:

$$\mu_t^{SAS} \geq \mu_t^{LES} \tag{27}$$

Where μ_t^{SAS} is the eddy-viscosity of SST-SAS model and the μ_t^{LES} is the eddy-viscosity of Smagorisnky model.

In fact, there exists considerable areas where L_{vk} is smaller than local grid scale. As a result, the eddy-viscosity of SST-SAS model is substituted with the eddy-viscosity of Smagorinsky model. Hence, the characteristics of Smagorinsky model is supposed to substantially influence the performance of SST-SAS. To preliminarily investigate the effect of the L_{vk} limiter on SST-SAS, here modifies the value of the Smagorsinky constant $C_s = 0.11$ contained in the L_{vk} limiter to be $C_s = 0.08$. It can be seen form Fig. 12 that the performance of mean pressure coefficient is better, which is closer to the experimental result.

The SST-SAS model has a pure URANS nature and the joint of the RANS region and the LES-like region is dependent on the characteristic

of flowfiled. At the very beginning of simulation, SST-SAS demonstrates near two-dimensional(2D) turbulence structure, which can be described as "RANS-like" behavior, when the L_{vk} is so large that the Q_{SAS} term is nonactivated. Then along with the unsteadiness develops in the flowfield, L_{vk} decreases and Q_{SAS} increases so that smaller turbulence scales can be resolved and more evident 3D effect can be simulated as can be seen in Fig. 13

From the previous model construction, we can see that the SAS model introduces the von Karman length scale L_{vk} to control the generation of the source term Q_{SAS} in the ω transport equation by the proportional relationship between the local turbulence scale L and L_{vk}, so the SAS model increases the value of ω in the separation region by the regulation of L/L_{vk}, and thus decreases the value of turbulent viscosity, see the Fig. 14.
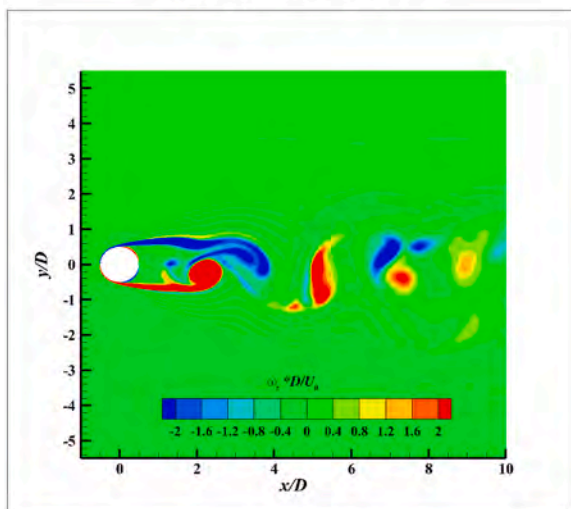
3.7.2. Discussion of SST-PANS model

The core of PANS model is the ratio between the local turbulence scale and the grid scale. Both of which are used to increase the value of ω by decreasing the amount of dissipative term in the ω equation, thus decreasing the turbulent viscosity. The PANS model is designed to
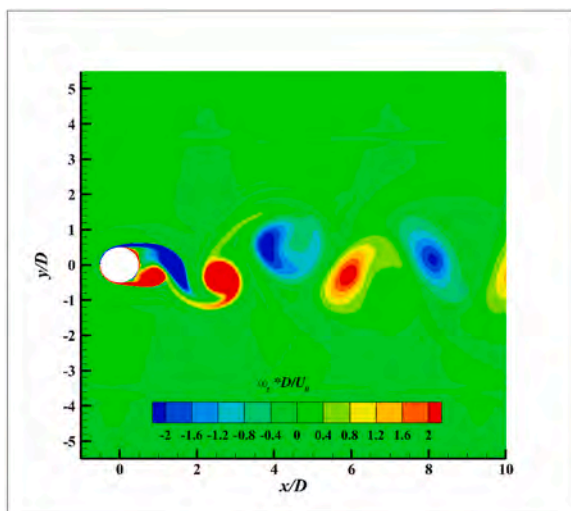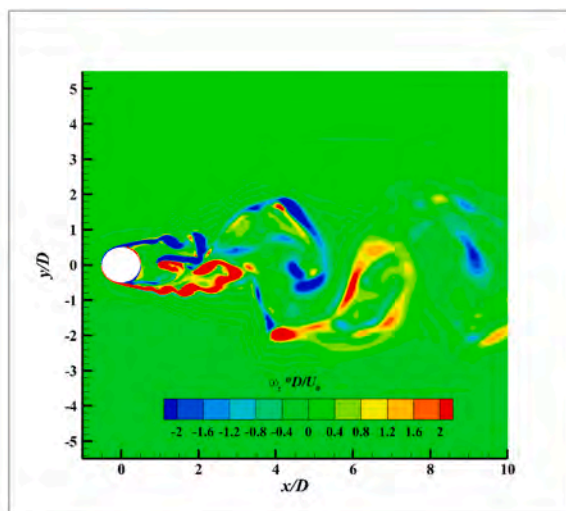
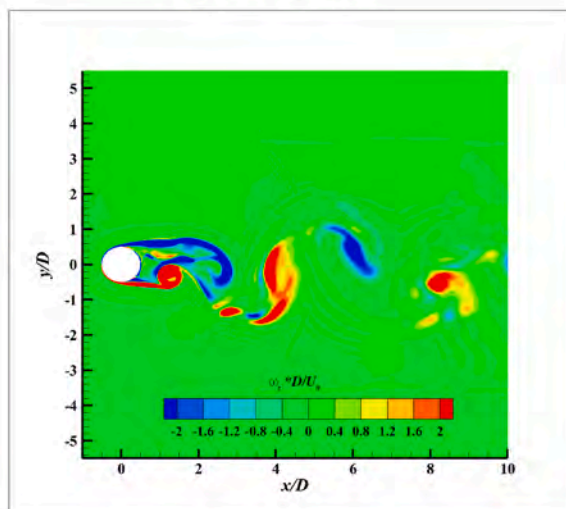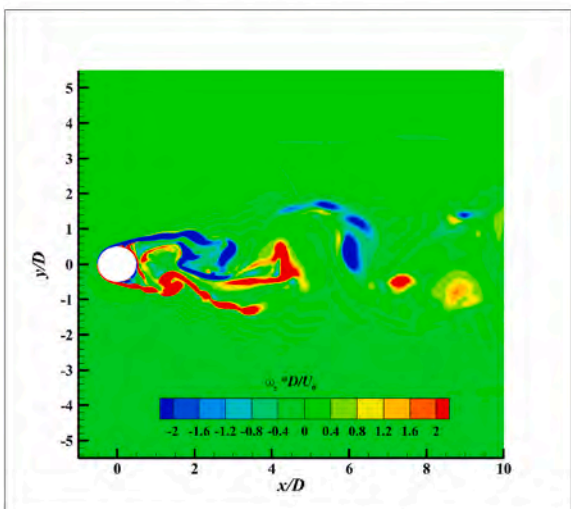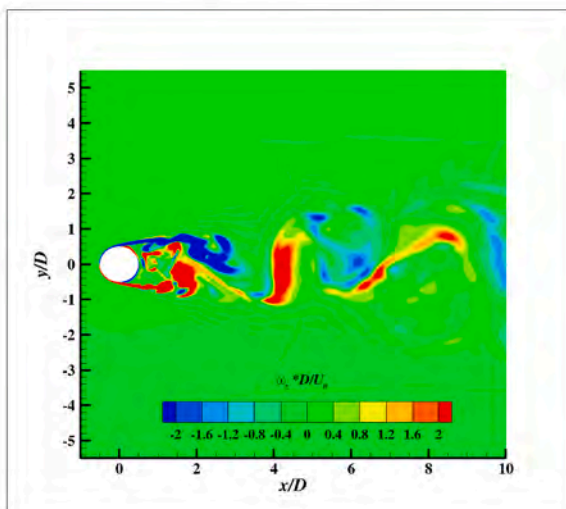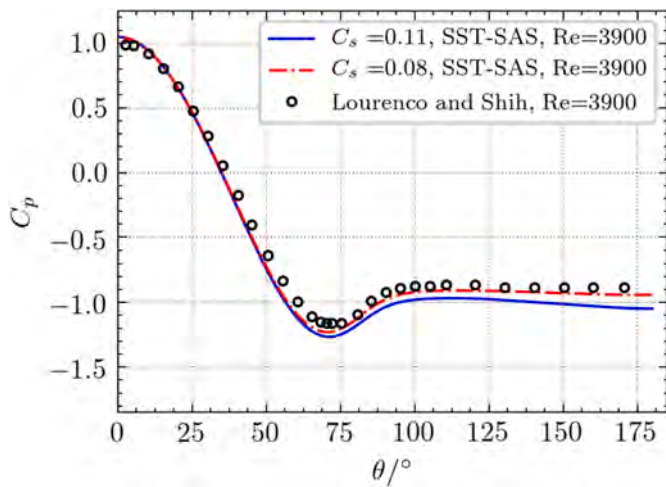**Fig. 11.** Isocontour maps of vorticity for the flow past a cylinder in horizontal plane $z/D = 0$.

Fig. 12. Cp distributions along the cylinder surface for SST-SAS.(θ=0° corresponding to the front stagnation point).
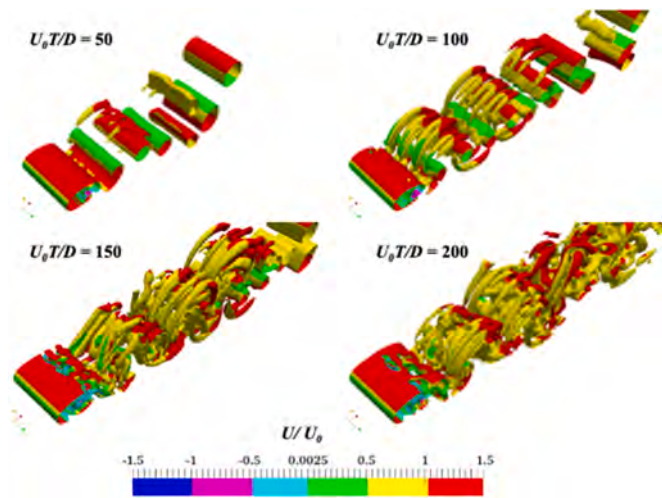

Fig. 13. Isocontour of the 3D vortex structures simulated by SST-SAS.

regulate the ratio of solvable/non-solvable turbulence by adding an fk parameter, the smaller the fk value, the more solvable scales are released.

Fig. 15 displays the surface pressure Cp distributions around the circular cylinder for SST-PANS model. We compare the calculations from different modeling strategies with the experiment of conducted by

Lourenco and Shih(Lourenco, 1994) at the same Reynolds number (Re = 3900). The present SST-PANS computations with fk = 0.1 and variable fk give good agreement with the experimental data. The prediction from SST-IDDES is also satisfactory, whereas the computed Cp distributions from PANS with fk = 1.0 show large deviations from the experiment.

Fig. 16 presents instantaneous view of coherent vortex structures contoured by using Omega-liutex Ω_{Liu}. The vortical structures resolved by f_k=1.0 are very coarse and like RANS models. More fine-scale structures are resolved as expected when the value of f_k is 0.1. The formation of Kelvin-Helmholtz instabilities in the very near wake are clearly observed in the simulations of PANS with f_k = 0.1 as the separated laminar shear layers convect downstream. The vortical structures resolved by variable f_k PANS are close to other hybrid models. The viscosity distribution in Fig. 11(d) shows that the turbulent viscosity decreases due to the encryption of the grid in the near-wall region, which leads to the decrease of the Reynolds stress of the modelling, and at the same time there is no sufficient Reynolds stress to solve for, leading to the phenomenon of Reynolds stress deficiency, which also verifies the defect that the SST-PANS model is more sensitive to the grid.

3.7.3. Discussion of SST-IDDES model

Fig. 17 shows the evolution of instantaneous vorticity Z in one vortex shedding cycle. The formation of the free shear layers from the cylinder surface took place identically for all runs. As the boundary layers from the upper and lower parts of the cylinder surface detach, free-shear layers are formed. The separating shear layers behind the cylinder become unstable, and small-scale vortices can be clearly observed in the
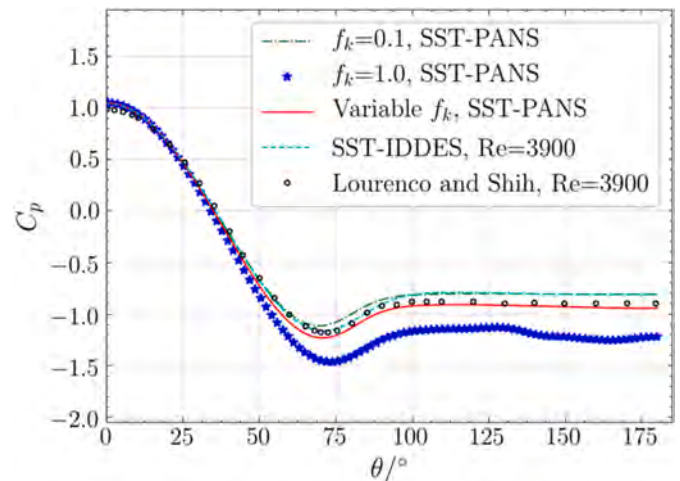

Fig. 15. Cp distributions along the cylinder surface for SST-PANS.(θ=0° corresponding to the front stagnation point).
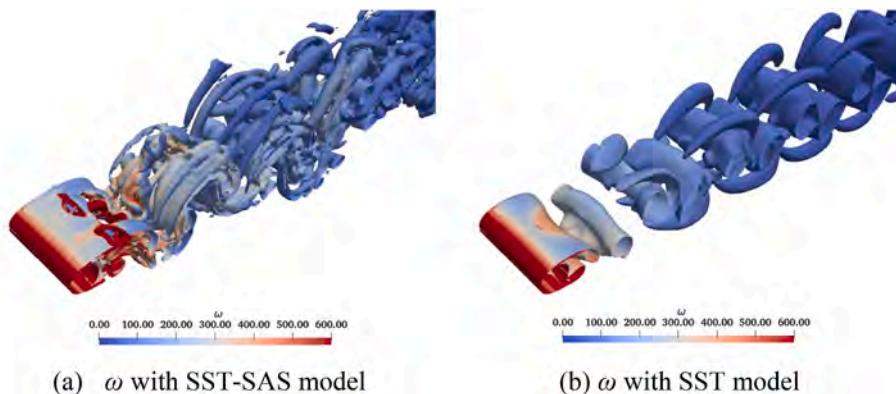

(a) ω with SST-SAS model

(b) ω with SST model

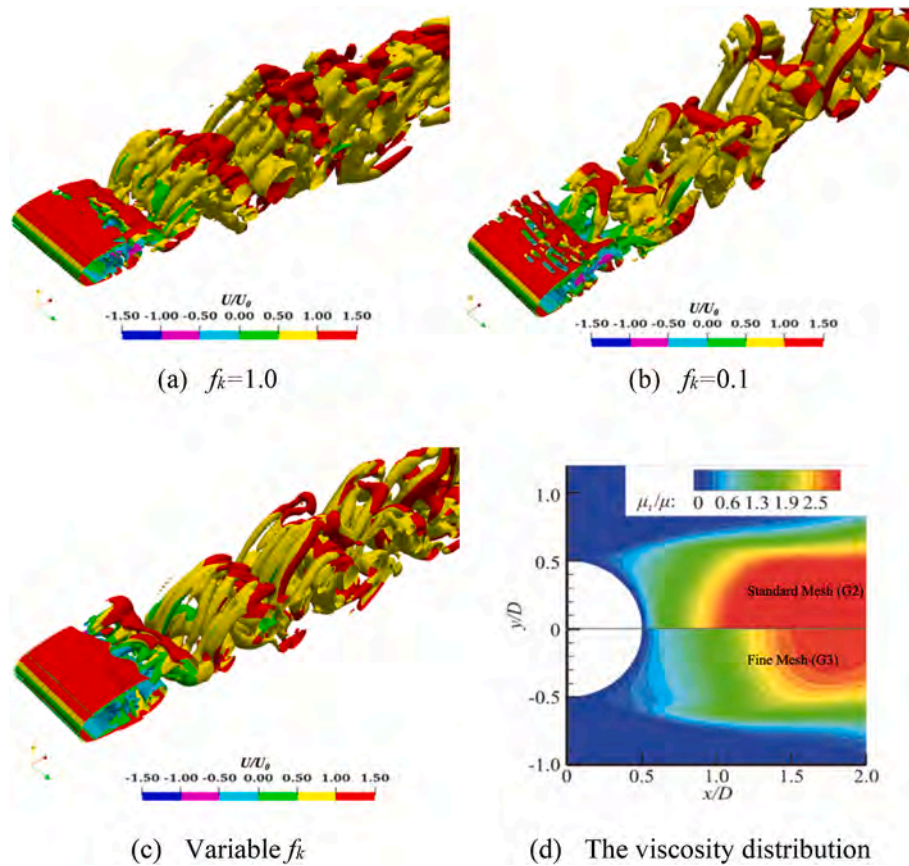**Fig. 14.** Isocontour of the 3D vortex structures and ω in the separation region.

Fig. 16. Instantaneous view of coherent vortex structures contoured by using Omega-liutex Ω_{Liu}: (a) f_k=1.0; (b) f_k=0.1; (c) variable f_k; (d) The viscosity distribution (variable f_k).

shear layers.

Fig. 18 shows mean velocities in different cross-stream profiles (x/D, y/D, z/D) = (1.06, 0, 0), (1.54, 0, 0), (2.02, 0, 0) of downstream. At (x/D, y/D, z/D) = (1.06, 0, 0), the axial velocity profile exhibits a typical U shape that many others have also found in their DNS studies(Frederic, 2002) At (x/D, y/D, z/D) = (1.54, 0, 0)and (x/D, y/D, z/D) = (2.02, 0, 0), it can be seen that the mean flow velocity in the near wake region evolves toward a V-shape further downstream. These profiles of the mean streamwise velocity for both turbulence models are consistent with the observations made earlier with regard to the length of the recirculation bubble. It has been discussed by Kravchenko(Kravchenko and Moin, 2000) that the difference between a U shape and a V shape of the mean streamwise velocity profile in the near wake is mainly due to the shear layer dynamics which affect this region. It is worth noting that the mean flow velocities obtained from the SST-IDDES model at three downstream locations is most consistent with the PIV results of Parnaudeau et al. (2008).

The mean transverse velocity profiles at three downstream locations (x/D, y/D, z/D) = (1.06, 0, 0), (1.54, 0, 0), (2.02, 0, 0) in the cylinder's wake are also shown Fig. 19. It can be seen that the SST and LES results differ most from the Parnaudeau et al. (2008)experimental values. When it is compared to the experimental results, the results of $k-\omega$ SST RANS model is larger, while the LES results shows smaller results. It can be seen that the velocity profiles obtained by SST-IDDES models show a high accuracy in comparison with the experimental values of Parnaudeau. There are some errors in the velocity patterns and peaks of other models.

The normalized mean stream-wise velocity $\bar{u}/U_0$ in the far wake of the cylinder ($x/D \leq 10$) is plotted in Fig. 20. Obviously, SST didn't predicts the minimum value along the centerline of the cylinder. It can be seen that the calculated results of the hybrid turbulence model SST-

IDDES are closer to the experimental results than other models, while the minimum value of the flow velocity predicted by RANS is lower than the experimental results, most obviously at the three cross sections (x/D, y/D, z/D) = (6.0, 0, 0), (7.0, 0, 0), (10.0, 0, 0). The reason for this phenomenon can be that the turbulent dissipation calculated by RANS is too large, resulting in the vortices being dissipated prematurely as they develop downstream. In contrast, the turbulence dissipation calculated by the hybrid model is closer to the real situation, so the vortex can still be maintained at a distance downstream without being completely dissipated.

3.7.4. Discussion of increasing Reynolds number

When increasing the value of Reynolds number, we get overall flow parameters of the flow past a circular cylinder at higher Reynolds number Re = 140000.

Summary of the global flow quantities for circular cylinder flow is listed in Table 5. Based on the results listed in Table 5, it was concluded that the values obtained by the SST-PANS and SST-IDDES are in good agreement with the experimental data (Cantwell and Coles, 1983). Comparing the mean surface pressure coefficient of SST-PANS,SST-SAS and SST-IDDES models with experimental results, the SST-IDDES models appear to be in better agreement with experimental results than the SST-PANS and SST-SAS turbulent model.

4. Conclusions

Based on the OpenFOAM open-source platform, this paper presents the numerical simulation of the flow around cylinder using hybrid turbulence models, and gives the time-averaged statistical analysis and comparison with the experiments in the literature. To compare the capability of SST-PANS,SST-SAS and SST-IDDES to predict the massively
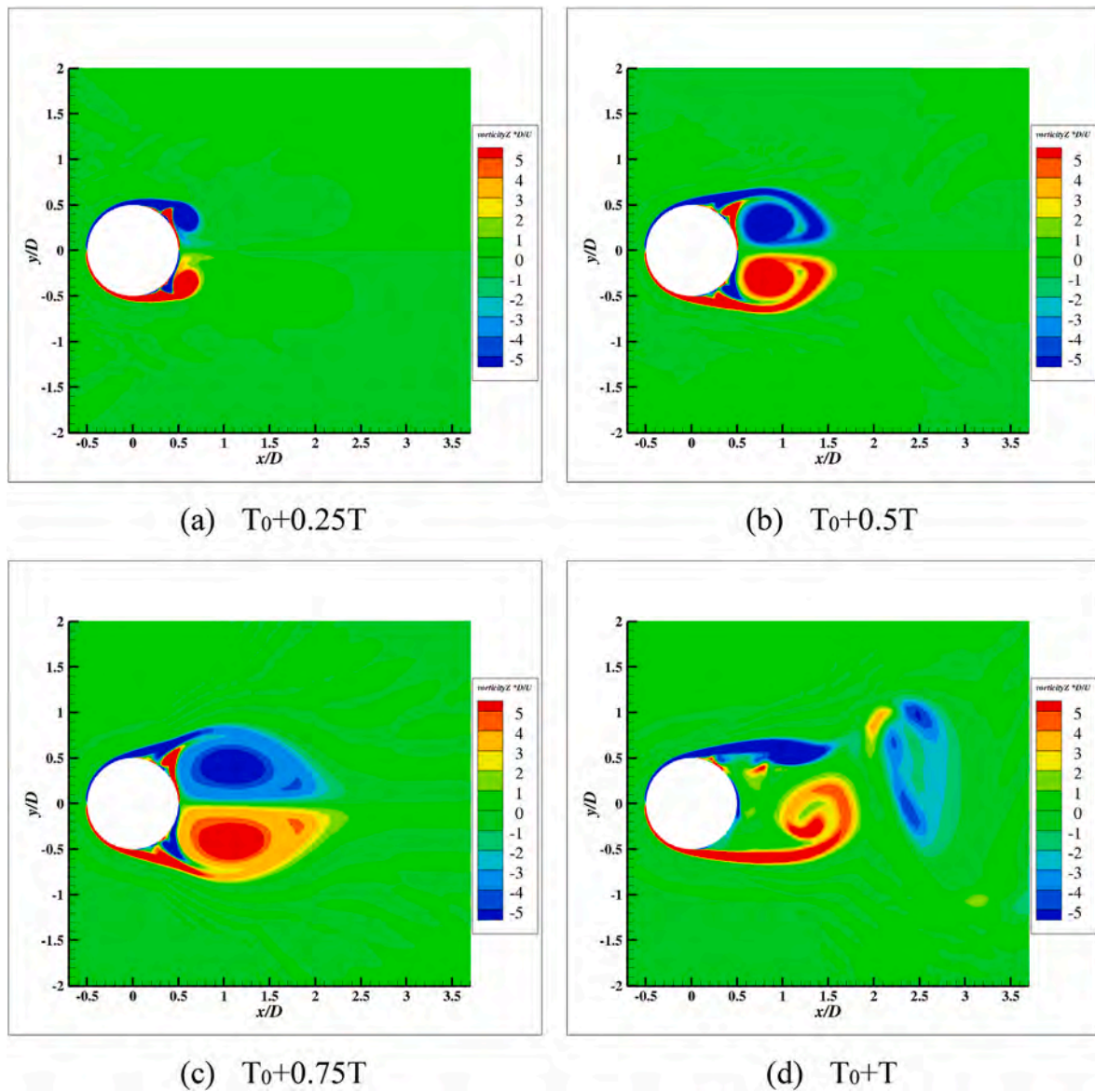
(a) $T_0+0.25T$ (b) $T_0+0.5T$

(c) $T_0+0.75T$ (d) T_0+T

Fig. 17. Isocontour maps of vorticity at horizontal plane $z/D = 0$ in one vortex shedding cycle.
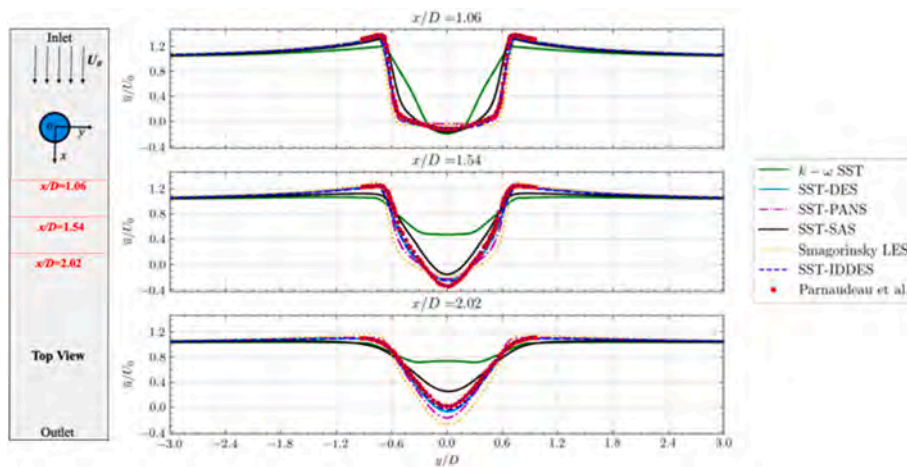

Fig. 18. Mean streamwise velocity profiles at three downstream locations in the near wake for a single cylinder at $Re = 3900$.
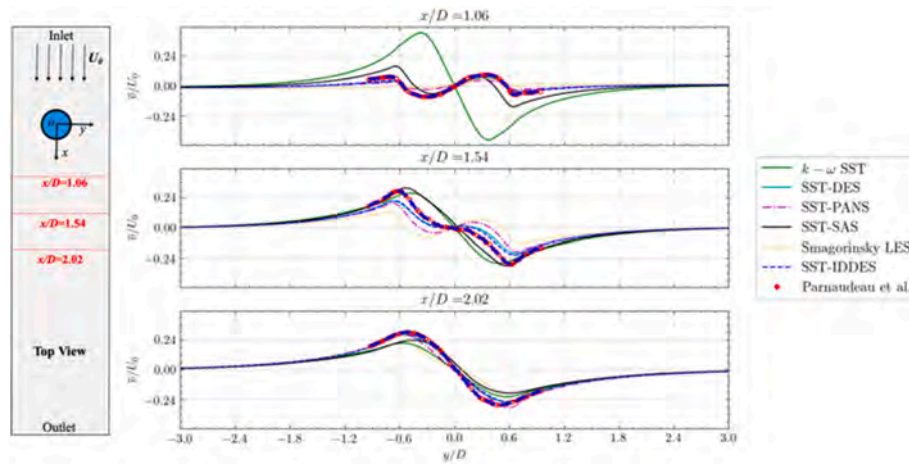
Fig. 19. Mean transverse velocity profiles at three downstream locations in the near wake for a single cylinder at *Re* = 3900.
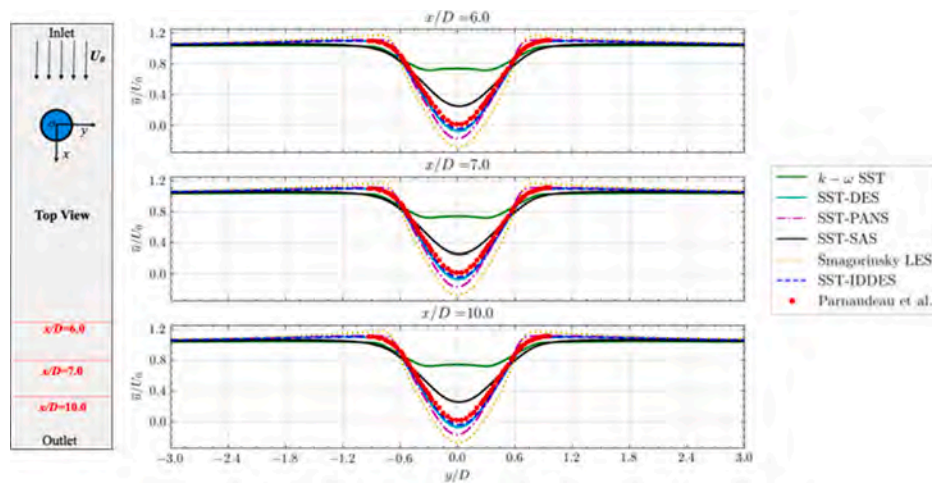

Fig. 20. Mean streamwise velocity profiles at three downstream locations in the far wake for a single cylinder at *Re* = 3900.

Table 5
Overall flow parameters of the flow past a circular cylinder, Reynolds number (*Re*) Re = 140000.

Data Source	$\overline{C_d}$	C_{l-rms}	C_{pb}	S_t
Experiment (Cantwell and Coles, 1983)	1.24	–	1.02	0.179
Present SST-PANS (variable f_k)	1.31	0.65	1.29	0.201
Present SST-SAS (C_s = 0.11)	1.14	0.69	1.25	0.203
Present SST-IDDES	1.22	0.61	0.96	0.181

separated flow, a 3D flow past a circular cylinder at subcritical Reynolds number Re = 3900 is numerically studied. The following main conclusions can be drawn from the analysis of the vortex characteristics of the flow field.

(1) The analysis of drag coefficient C_d, cylindrical wake pressure coefficient C_p and S_t number, dimensionless return region length and dimensionless minimum incoming velocity min U/U_0 shows that the results of the hybrid turbulence models (SST-SAS, SST-PANS, SST-IDDES models) are in good agreement with the experimental values, while the results of the RANS model are not so.

(2) Moreover, both these hybrid models are able to simulate small turbulence structures and 3D effect even though their hybrid mechanisms are quite different. However, compared with SST-IDDES, the SST-SAS and SST-PANS both affected by parameters when it comes to accurate prediction, meaning that SST-SAS and SST-PANS still remains improvements. Both SAS and PANS are able to solve more turbulent scales by reducing the turbulent viscosity of the flow field, but SAS and PANS have completely different mechanisms for regulating the solution scales. Interestingly, when the constant C_s = 0.11 contained in the L_{vk} limiter is modified to be C_s = 0.08, SST-SAS is also able to achieve better performance in the same mesh. This observation stimulates the need to investigate how the L_{vk} limiter influences the performance of SST-SAS.

(3) The analysis of velocity profiles at different locations behind the cylinder further shows that the hybrid model is closer to the experimental results than RANS, and SST-IDDES has an advantage over other models in numerically simulating the non-constant large separation flow problem. The analysis of the vortex structure of the cylindrical transient flow field shows that the RANS method only modulates large vortices, which generates too much vortex viscosity and thus "suppresses" the formation of 3D fine vortex structure, while the hybrid model can calculate and simulate the 3D vortex structure well, which is closer to the real physical phenomenon. The SST-IDDES model has the best simulation results.

CRediT authorship contribution statement

Jiawei He: Data curation, Writing – original draft, preparation,

Visualization, Investigation, Software, Validation. **Wentao Wang:** Visualization, Investigation, Validation. **Weiwen Zhao:** Software, Data curation, Visualization, Investigation, Validation. **Decheng Wan:** Supervision, Conceptualization, Methodology, Investigation, Writing – review & editing.

Declaration of competing interest

The authors declare the following financial interests/personal relationships which may be considered as potential competing interests:

Data availability

Data will be made available on request.

Acknowledgements

References

Cantwell, B., Coles, D., 1983. An experimental study of entrainment and transport in the turbulent near wake of a circular cylinder. J. Fluid Mech. 136, 321. https://doi.org/10.1017/S0022112083002189.

D'Alessandro, V., Montelpare, S., Ricci, R., 2016. Detached–eddy simulations of the flow over a cylinder at Re = 3900 using OpenFOAM. Comput. Fluids 136, 152–169. https://doi.org/10.1016/J.COMPFLUID.2016.05.031.

Elmiligui, A., Abdol-Hamid, K., Massey, S., Pao, S., 2004. Numerical study of flow past a circular cylinder using RANS, hybrid RANS/LES and PANS formulations. In: 22nd Applied Aerodynamics Conference and Exhibit. American Institute of Aeronautics and Astronautics, Reston, Viriginia. https://doi.org/10.2514/6.2004-4959.

Frederic, T., 2002. Direct and Large-Eddy Simulation of Flow Around a Circular Cylinder at Subcritical Reynolds Numbers. Univ. der TU München. Fakultät für Maschinenwesen.

Gao, Y., Liu, C., 2018. Rortex and comparison with eigenvalue-based vortex identification criteria. Phys. Fluids 30, 085107. https://doi.org/10.1063/1.5040112.

Gritskevich, M.S., Garbaruk, A.V., Schütze, J., Menter, F.R., 2012. Development of DDES and IDDES formulations for the k-ω shear stress transport model. Flow, Turbul. Combust. 88, 431–449. https://doi.org/10.1007/s10494-011-9378-4.

Heinz, S., 2020. A review of hybrid RANS-LES methods for turbulent flows: concepts and applications. Prog. Aero. Sci. 114, 100597 https://doi.org/10.1016/j.paerosci.2019.100597.

Khan, N.B., Ibrahim, Z., Bin Mohamad Badry, A.B., Jameel, M., Javed, M.F., 2019. Numerical investigation of flow around cylinder at Reynolds number = 3900 with large eddy simulation technique: effect of spanwise length and mesh resolution. Proc. Inst. Mech. Eng. Part M J. Eng. Marit. Environ. 233, 417–427. https://doi.org/10.1177/1475090217751326.

Krappel, T., Kuhlmann, H., Kirschner, O., Ruprecht, A., Riedelbauch, S., 2015. Validation of an IDDES-type turbulence model and application to a Francis pump turbine flow simulation in comparison with experimental results. Int. J. Heat Fluid Flow 55, 167–179. https://doi.org/10.1016/j.ijheatfluidflow.2015.07.019.

Kravchenko, A.G., Moin, P., 2000. Numerical studies of flow over a circular cylinder at ReD=3900. Phys. Fluids 12, 403–417. https://doi.org/10.1063/1.870318.

Krishnan, V., Squires, K.D., Forsythe, J.R., 2006. Prediction of the flow around a circular cylinder at high Reynolds number. In: 44th AIAA Aerospace Sciences Meeting and Exhibit, 9-12 January 2006. Reno, Nevada ,United States, pp. 10765–10774.

Liu, C., Gao, Y.S., Dong, X.R., Wang, Y.Q., Liu, J.M., Zhang, Y.N., Cai, X.S., Gui, N., 2019. Third generation of vortex identification methods: Omega and Liutex/Rortex based systems. J. Hydrodyn. 31, 205–223. https://doi.org/10.1007/s42241-019-0022-4.

Lourenco, L.S.C., 1994. Characteristics of the Plane Turbulent Near Wake of a Circular Cylinder. Technical Report TF-62. CTR Annual Research Briefs,NASA Ames/Stanford University.

Lysenko, D.A., Ertesvåg, I.S., Rian, K.E., 2012. Large-eddy simulation of the flow over a circular cylinder at Reynolds number 3900 using the openfoam toolbox. Flow. Turbul. Combust. 89, 491–518. https://doi.org/10.1007/s10494-012-9405-0.

Menter, F.R., 1994. Two-equation eddy-viscosity turbulence models for engineering applications. AIAA J. 32, 1598–1605. https://doi.org/10.2514/3.12149.

Menter, F.R., Egorov, Y., 2010. The scale-adaptive simulation method for unsteady turbulent flow predictions. Part 1: theory and model description. Flow, Turbul. Combust. 85, 113–138. https://doi.org/10.1007/s10494-010-9264-5.

Menter, F.R., Kuntz, M., Langtry, R., 2003. Ten years of industrial experience with the SST turbulence model. Turbul. Heat Mass Transf. 4 4, 625–632. https://doi.org/10.4028/www.scientific.net/AMR.576.60.

Mockett, C., Haase, W., Thiele, F., 2015. Go4hybrid: a European initiative for improved hybrid RANS-LES modelling. Notes Numer. Fluid Mech. Multidiscip. Des. 130, 299–303. https://doi.org/10.1007/978-3-319-15141-0_24.

Mockett, C., Perrin, R., Reimann, T., Braza, M., Thiele, F., 2010. Analysis of detached-eddy simulation for the flow around a circular cylinder with reference to PIV data. Flow, Turbul. Combust. 85, 167–180. https://doi.org/10.1007/s10494-009-9243-x.

Parnaudeau, P., Carlier, J., Heitz, D., Lamballais, E., 2008. Experimental and numerical studies of the flow over a circular cylinder at Reynolds number 3900. Phys. Fluids 20, 085101. https://doi.org/10.1063/1.2957018.

Pereira, F.S., Vaz, G., Eça, L., Girimaji, S.S., 2018. Simulation of the flow around a circular cylinder at Re =3900 with Partially-Averaged Navier-Stokes equations. Int. J. Heat Fluid Flow 69, 234–246. https://doi.org/10.1016/j.ijheatfluidflow.2017.11.001.

Razi, P., 2017. Partially-averaged Navier-Stokes (PANS) Method for Turbulence Simulations: Near-Wall Modeling and Smooth-Surface Separation Computations.

Shur, M., Spalart, P.R., Strelets, M., Travin, A., 2011. A rapid and accurate switch from rans to les in boundary layers using an overlap region. Flow, Turbul. Combust. 86, 179–206. https://doi.org/10.1007/s10494-010-9309-9.

Shur, M.L., Spalart, P.R., Strelets, M.K., Travin, A.K., 2014. Synthetic turbulence generators for RANS-LES interfaces in zonal simulations of aerodynamic and aeroacoustic problems. Flow. Turbul. Combust. 93, 63–92. https://doi.org/10.1007/s10494-014-9534-8.

Shur, M.L., Spalart, P.R., Strelets, M.K., Travin, A.K., 2008. A hybrid RANS-LES approach with delayed-DES and wall-modelled LES capabilities. Int. J. Heat Fluid Flow 29, 1638–1649. https://doi.org/10.1016/j.ijheatfluidflow.2008.07.001.

Spalart, P., 2000. Strategies for turbulence modelling and simulations. Int. J. Heat Fluid Flow 21, 252–263. https://doi.org/10.1016/S0142-727X(00)00007-2.

Stamou, A.I., Papadonikolaki, G., 2014. Modeling the 3-d flow around a cylinder using the SAS hybrid model. Glob. Nest J. 16, 901–918. https://doi.org/10.30955/gnj.001443.

Tian, S., Gao, Y., Dong, X., Liu, C., 2018. Definitions of vortex vector and vortex. J. Fluid Mech. 849, 312–339. https://doi.org/10.1017/jfm.2018.406.

Wissink, J.G., Rodi, W., 2008. Numerical study of the near wake of a circular cylinder. Int. J. Heat Fluid Flow 29, 1060–1070. https://doi.org/10.1016/J.IJHEATFLUIDFLOW.2008.04.001.

Xu, C., Chen, L., Lu, X., 2007. Large-Eddy and Detached-Eddy Simulations of the separated flow around a circular cylinder. J. Hydrodyn. 19, 559–563. https://doi.org/10.1016/s1001-6058(07)60153-x.

Ye, W., Luo, X., Li, Y., 2020. Modified partially averaged Navier–Stokes model for turbulent flow in passages with large curvature. Mod. Phys. Lett. B 34, 2050239. https://doi.org/10.1142/S0217984920502395.

Zhao, W., Wan, D., 2016. Benchmark for detached-eddy simulation of flow past tandem cylinders. Elev. Asian Comput. Fluid Dyn. Conf. Sept. 16–20, 2016, Dalian, China 397–401.

Zhao, W., Zou, L., Wan, D., Hu, Z., 2018. Numerical investigation of vortex-induced motions of a paired-column semi-submersible in currents. Ocean Eng. 164, 272–283. https://doi.org/10.1016/j.oceaneng.2018.06.023.